Multi-object Segmentation with Coupled Deformable Models

Dagmar Kainmueller[a], Hans Lamecker[a], Stefan Zachow[a], Markus Heller[b], Hans-Christian Hege[a*]

[a]Zuse Institute Berlin, Takustr. 7, 14195 Berlin, Germany
[b]Julius Wolff Institut and Center for Musculoskeletal Surgery, Charité - Universitätsmedizin Berlin, Germany

Abstract. For biomechanical simulations, the segmentation of multiple adjacent anatomical structures from medical image data is often required. If adjacent structures are hardly distinguishable in image data, automatic segmentation methods for single structures in general do not yield sufficiently accurate results. To improve segmentation accuracy in these cases, knowledge about adjacent structures must be exploited. Optimal graph searching based on deformable surface models allows for a simultaneous segmentation of multiple adjacent objects. However, this method requires a correspondence relation between vertices of adjacent surface meshes. Line segments, each containing two corresponding vertices, may then serve as shared displacement directions in the segmentation process. In this paper we propose a scheme for constructing a correspondence relation in adjacent regions of two arbitrary surfaces. When applying the thus generated shared displacement directions in segmentation with deformable surfaces, overlap of the surfaces is guaranteed not to occur. We show correspondence relations for regions on a femoral head and acetabulum and other adjacent structures, as well as preliminary segmentation results obtained by a graph cut algorithm.

1 Introduction

For patient-specific biomechanical simulations, e.g. of the human lower limb, an accurate reconstruction of the bony anatomy from medical image data is required. This particularly applies to joint regions, as simulation results heavily depend on the location of joints [1]. In CT data, bony tissue can usually be reconstructed by simple thresholding. However, in joint regions, thresholding is often not sufficient for separating adjacent individual bones from each other. Due to large slice thickness or pathological changes of the bones, the joint space may be hard to detect even for a human observer. Fig. 1a and 1b show exemplary situations.

We can achieve good initializations for individual (single) bony structures (e.g. pelvis, femur) by our segmentation framework which is based on statistical shape models (SSM) and free form models (FFM) [2]. Segmentations with SSMs yield good initializations, but lack precision, since previously unknown patient-specific anatomy is generally not contained in the model. With FFMs more precise segmentations can be achieved, but they suffer from a loss of shape knowledge, causing inaccurate interpolations where the object to be segmented cannot be distinguished from adjacent structures in image data. Furthermore, the lack of image information may generally lead to overlapping segmentation results when adjacent structures are segmented separately.

A basic idea for improving segmentation results and simultaneously solving the overlap problem is to segment multiple adjacent objects at the same time and incorporate some knowledge about their spatial relationship. The problem we address in this paper is how to establish a suitable coupling of two arbitrary adjacent deformable surface models (triangular meshes), assuming that a good initialization of the two models is given. The contribution of this work is a construction scheme for shared displacement directions for two arbitrary surfaces, that is, line segments along which vertices of both surfaces can be displaced in a deformable surface segmentation framework. We used the coupling realized by these shared displacement directions for fine grain multi-object segmentation based on graph cuts. This paper presents a proof of concept with very encouraging results.

2 Related Work

Costa et al. [3] employ a non-overlapping constraint for coupled segmentation of prostate and bladder with deformable models. They propose a force that drives two models apart if intersections occur in the segmentation process. This method principally allows for free form deformations of the models while coping with overlap. If present, a statistical shape model can be enforced on one of the models. If one structure is better distinguishable from the background than the other, an asymmetric non-overlap force can be applied. This approach yields promising results in prostate and bladder segmentation. However, displacements are not found *simultaneously* for both objects: Apart from the non-overlap force which only exists if an overlap has already occurred, one object does not take into account any knowledge about the presence of the other object in displacement computation.

* {kainmueller, lamecker, zachow, hege}@zib.de

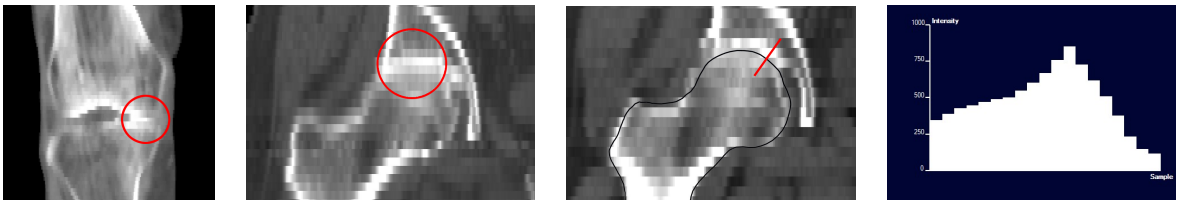

(a) (b) (c) (d)

Figure 1. (a) CT data of distal femur and proximal tibia, slice thickness 2mm, (b) acetabulum and proximal femur, slice thickness 4,6mm. Joint space hardly visible in encircled areas. (c) Acetabulum and proximal femur, slice thickness 5mm, with surface model cross-section (black) and domain of intensity profile (line segment). (d) Intensity profile for domain in (c).

Tsai et al. [4] build composite statistical shape models by applying principal component analysis to a training set of implicit (signed distance function) representations of multiple objects. They apply such models to the segmentation of subcortical brain structures and male lower abdominal structures (prostate gland, rectum, obturator muscles). Babalola et al. [5] build a composite active appearance model on the basis of explicit (surface-mesh) representations of multiple subcortical brain structures. They apply this model to obtain a good initialization of brain structure models to accurately segment the caudate in a single object segmentation framework. Composite statistical shape models yield a tight coupling of the deformations of multiple objects. Ideally, no overlap between adjacent objects should be possible in model space. Anyway, neither of the two approaches allows for a fine grain free form multi-object segmentation, as model deformation is bound to the respective shape space.

Li et al. [6] solve the overlap problem with optimal graph searching in a deformable model segmentation framework. They apply their method to the segmentation of bone and cartilage in 3D MRI of human ankles. Vertex normals of the bone surface are used as shared displacement directions for bone and cartilage surfaces. Thus, one direction may be used to search for two object boundaries, thereby allowing for a completely simultaneous segmentation process. Methods involving shared displacement directions have been described for surfaces on which corresponding vertices are easily found. This holds for height field or cylindrical surfaces in regular grids [7], or if one surface can be obtained by displacing the other along its vertex normals [6]. However, to the best of our knowledge, there is at present no way for generating shared displacement directions on arbitrary surfaces.

3 Multi-object segmentation with graph cuts

In segmentation with deformable surfaces, *intensity profiles* at each vertex of the surface mesh are commonly used to guide the deformation process. An intensity profile is a set of intensity samples taken from image data along a line segment at a vertex of the surface mesh, see Fig. 1c and 1d. Note that the term *intensity profile* or just *profile* may be used as referring to the sampled intensities only, yet we use it to refer to the domain of the sampling, i.e. a line segment, as well. Fig. 2a shows exemplary profiles on a triangular surface mesh. Profiles are commonly defined to run along vertex normals, but other directions may be chosen as well. On each profile, a cost function is derived from image data for a number of equidistant sampling points. The minimum cost sample point on a profile may serve as a desired (locally optimal) position for the respective vertex.

However, graph cut algorithms allow for a *global* optimization of the sum of costs for each vertex displacement while respecting hard constraints on the distance of multiple objects and on single object smoothness. Multiple surfaces can be coupled with *shared intensity profiles* at individual vertices. Minimum and maximum distance constraints can be enforced on the new vertex positions that graph optimization finds for each surface on each shared profile. For more details on graph construction see [7]. The optimization problem can be solved in polynomial time, as discussed in [8].

4 Non-overlapping surface deformations

Before shared profiles can be constructed, surface models of adjacent structures must be initialized to have a reasonable spatial relation to each other. For bony structures of the lower limb we can achieve initializations in CT data with a maximum surface distance of about 1cm to a manual expert segmentation. For two such well-initialized surface models, we identify a potential overlap region by inflating each surface by a user-defined amount l (Fig. 2b and 2c). Our concern is to couple the surfaces with shared profiles wherever single profiles of length $2l$ would reach the overlap region.

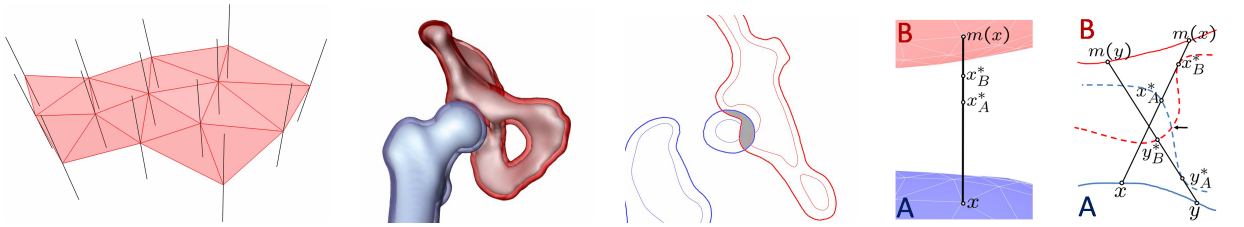

(a) (b) (c) (d) (e)

Figure 2. (a) Triangular surface mesh with profiles in normal direction. (b) Proximal femur and ilium. Transparent: isosurfaces in distance transforms. (c) 2D cross-section. Thin lines: surface contours. Thick: isosurface contours. Grey: potential overlap region. (d) Necessary condition: x_A^* lies closer to x than x_B^*. (e) Contours A, B. Black lines: Connections of mapped points intersect. Dotted: Exemplary deformed contours, intersecting at black arrow.

4.1 Properties of shared intensity profiles

Which conditions must hold on shared profiles to generally prevent any overlap after surface deformation? Note one necessary condition posed on new vertex positions of coupled surface meshes A and B: Let x be a vertex on A and $m(x)$ the corresponding vertex on B. Then the new position x_A^* of x must lie closer to A than the new position x_B^* of $m(x)$ in profile direction, i.e. $\|x_A^* - x\| < \|x_B^* - x\|$ (if we disregard that surfaces can completely swap sides along shared profiles). See Fig. 2d. In the following we assume that this condition holds.

In 2D, when establishing shared profiles between deformable contours A and B, intersecting profiles can cause overlap of the deformed contours, as illustrated in Fig. 2e. Now we examine this situation in 3D. For this purpose we consider a bijective mapping m of piecewise *continuous* regions R_A and R_B on surfaces A and $B \subset \mathbb{R}^3$: Shared profiles on triangular meshes can be seen as a finite set of line segments connecting corresponding triangle vertices x and $m(x)$. Hence they partially define or are embedded in such a mapping. However, during surface deformation, not only each vertex, but *each point* on R_A and R_B is displaced along a line segment that leads to its corresponding point. Profiles may not intersect with each other, while other line segments that connect mapped point pairs do. Thus we are interested in properties of mappings m and not only in properties of shared profiles.

Overlap after surface deformation cannot occur if the mapping m satisfies what we call *non-intersection* condition, i.e. no two connections of two mapped point pairs intersect. For a proof, let R_A^* and R_B^* be the deformed regions. R_A^* is the image of a function f_A that maps each point x on R_A to a point x_A^* on the line segment $\{x + \lambda \cdot (m(x) - x) | 0 \leq \lambda \leq 1\}$. Each x_A^* is defined by an individual $\lambda_A(x) \in [0, 1]$. Likewise R_B^* is the image of f_B that maps each x on R_A to an $x_B^* = x + \lambda_B(x) \cdot (m(x) - x)$, with the additional constraint that $\lambda_A(x) < \lambda_B(x)$ for all $x \in R_A$. If the deformed regions intersect, we have $x, y \in R_A$ with $f_A(x) = f_B(x)$, i.e. $x + \lambda_A(x) \cdot (m(x) - x) = y + \lambda_B(y) \cdot (m(y) - y)$. The constraint $\lambda_A(x) < \lambda_B(x)$ implies $x \neq y$. This implies an intersection of the line segments $[x, m(x)]$ and $[y, m(y)]$. In reverse, if no two connections of two mapped point pairs intersect, the deformed regions do not intersect either. Note that the non-intersection condition also implies the continuity of m for homeomorphic regions R_A and R_B, yet continuity alone is not sufficient for preventing overlap.

4.2 Mapping of non-empty surface regions

The following scheme establishes a mapping of topologically equivalent regions on smooth, closed surfaces A and B that satisfies the non-intersection condition:

1. Compute the mid surface M (all points with same distance to A and B), and its normals n where possible.
2. Define finite length vectors v on M as follows: Scale normals n and inverse normals $-n$ to some length exceeding the maximum distance of any two points x on A and y on B. Then trim the scaled normals at the skeleton of M if they reach it. (The skeleton of a surface is the set of points that are centers of spheres that touch the surface in more than one point, but do not cut it.) The resulting vectors then do not intersect with each other.
3. Iteratively map points on A and B cut by the same vector v. Start with vectors on local minima of the signed euclidean distance function $d : M \to \mathbb{R}, x \mapsto d(x, A)$ on M. (Note that $d(x, A) = d(x, B)$ for all x.) Grow the regions considered on M as long as corresponding regions on A and B have the same topologies.

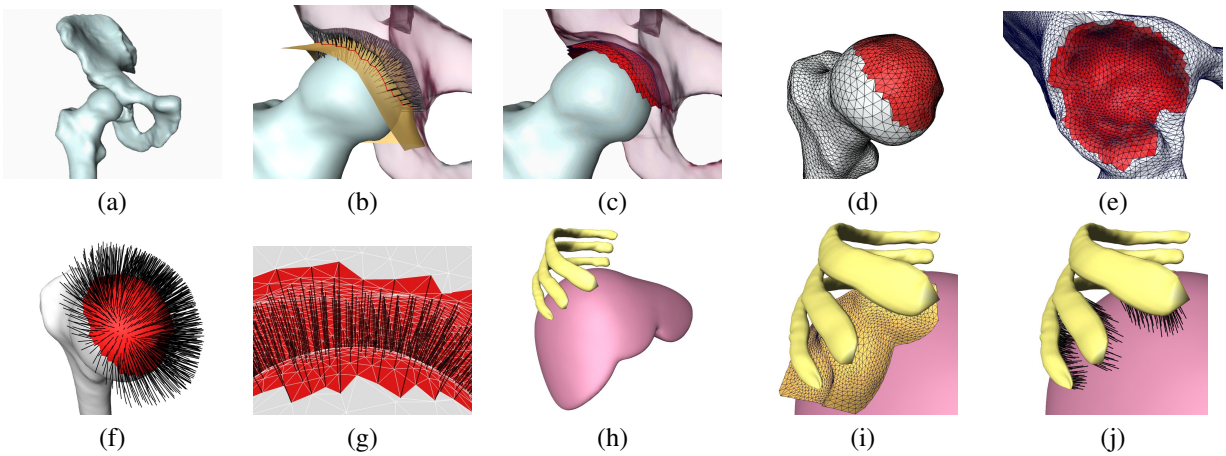

Figure 3. Construction of shared profiles. (a) Proximal femur and right ilium. (b) Mid surface (yellow) in region of interest, with normals entering both femur and illium. (c) Extracted region on mid surface (red). (d,e) surface meshes with integrated displaced region (red). (f,g) Vectors coupling femoral head and acetabulum. (h) Surface models of liver and nearby ribs. (i) Mid surface in region of interest. (j) Coupling vectors between liver and ribs.

This results in an intersection free mapping of regions. The mapping is not empty: At least all vectors defined on local minima of d connect corresponding points. Such local minima exist, as we are dealing with closed surfaces. The linear connections of the respective corresponding points do not contain any point of the skeleton of M. For a proof, see [9].

4.3 Generating shared intensity profiles

Based on the scheme for constructing an intersection-free mapping as proposed in Section 4.2, we realize a construction algorithm for shared profiles on pairs of adjacent *triangular* surfaces A and B. In the process, we modify the connectivity of parts of the surface meshes. The one-sided surface distance of the modified surface to the original surface is always zero. Concerning the reverse direction of the surface distance, no general assertions can be made.

Fig. 3 shows the construction pipeline for an exemplary femur and ilium. First, the mid surface M between the objects is computed as the zero level of the objects' distance transforms, subtracted from each other (Fig. 3b). M is discretized and triangulated to form a mesh of high regularity. The skeleton of M is approximated by uniformly displacing M along its surface normals in both directions and identifying self intersection points. Then we identify the region on M where its vertex normals, scaled to a user-specified maximal length, enter both femur and ilium, without reaching the skeleton of M first (Fig. 3b and 3c). This region is displaced onto each femur and ilium in vertex normal direction. Each displaced patch is merged into the respective surface mesh by removing all original triangles on the mesh which are surrounded by the patch boundary, and connecting the boundaries of remaining the mesh and the patch. Fig. 3d and 3e show the resulting surfaces.

As a result, we obtain a bijective mapping of the displaced (continuous) patches that satisfies the non-intersection condition. Thereby shared profiles between the modified surface meshes' vertices are defined, as shown in Fig. 3f and 3g. We let the shared profiles reach *into* the surfaces until they meet the skeleton of M, or the inner skeleton of the respective surface, or they reach a user-specified maximal length. As another example, Fig. 3h-3j show a liver model and a model of surrounding ribs which are connected. Three regions with shared profiles are identified here.

5 Results

In a first investigation we computed segmentations of a femoral head and ilium and a distal femur and proximal tibia in CT data with 5mm slice thickness (Fig. 4a). Single surface models were initialized individually with SSM fitting as described in [2]. Fig. 4b shows resulting initializations. Note the overlap of the initialized models. Shared profiles (Fig. 4c) were established as proposed in Section 4.3. A graph was then constructed as in [7], containing these shared profiles as well as traditional single profiles [2] in non-adjacent regions of the surfaces. We used thresholding in the image data (Fig. 4e) to derive a cost function on the profiles. Costs are low at sample points where intensities change from above to below the threshold, and high everywhere else. We applied the graph cut algorithm proposed in [8] to find optimal surfaces. Fig. 4d shows the resulting segmentations. The overlap was resolved and a reasonable interpolation was found in image regions where intensities lie above the threshold due to low image quality.

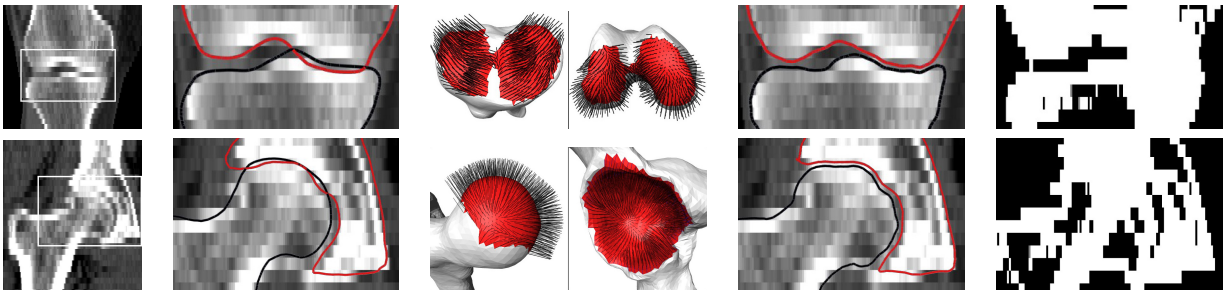

(a) (b) (c) (d) (e)

Figure 4. First row: Distal femur and proximal tibia. Second row: Acetabulum and proximal femur. (a) CT data with focus region (white boundary) for (b), (d), (e). (b) Model initialization with SSMs. (c) Shared profiles. (d) Graph optimization. (e) Threshold information used for model fitting.

6 Discussion

We proposed a method for coupling arbitrary adjacent surfaces by means of shared profiles. Two surfaces are guaranteed not to overlap if deformed along the shared profiles. Optimal graph searching on the graph obtained from the coupled surfaces produced encouraging segmentation results. The next task will be to evaluate segmentation results quantitatively on a set of 3D CT datasets by comparing them to manual expert segmentations. For this purpose, as a first step, variations among segmentations performed by different experts must be determined. This is of particular importance here as we are dealing with segmentations of adjacent objects which often are hardly distinguishable in image data, even for human observers. Until now, simple thresholding was performed for establishing a cost function. We are working on a more elaborate cost function design that considers more information (e.g. the gradient) contained in image data. We also plan to establish an automatic method for rough initialization of pelvis and femur models in CT datasets as starting positions for SSM segmentation. Until now, this first initialization requires manual interaction.

Acknowledgements

This work was initially presented at the International Symposium on Computational Models for Biomedical Simulation (ISBMS) 2008 in London, England [9]. D. Kainmueller is funded by DFG Collaborative Research Center SFB760. H. Lamecker is funded by DFG Research Center Matheon in Berlin. Thanks to Heiko Seim (ZIB) for providing the shape models of femur and tibia. Thanks to Charité Center for Musculoskeletal Surgery for providing the pelvis model.

References

1. M. Heller, G. Bergmann, G. Deuretzbacher et al. "Musculo-skeletal loading conditions at the hip during walking and stair climbing." *J Biomech* **34**, pp. 883–93, 2001.
2. D. Kainmueller, T. Lange & H. Lamecker. "Shape Constrained Automatic Segmentation of the Liver based on a Heuristic Intensity Model." In Heimann et al. [10], pp. 109–116.
3. M. J. Costa, H. Delingette, S. Novellas et al. "Automatic segmentation of bladder and prostate using coupled 3d deformable models." In N. Ayache, S. Ourselin & A. J. Maeder (editors), *MICCAI (1)*, volume 4791 of *Lecture Notes in Computer Science*, pp. 252–260. Springer, 2007.
4. A. Tsai, W. M. W. III, C. Tempany et al. "Coupled multi-shape model and mutual information for medical image segmentation." In C. J. Taylor & J. A. Noble (editors), *IPMI*, volume 2732 of *Lecture Notes in Computer Science*, pp. 185–197. Springer, 2003.
5. K. Babalola, V. Petrovic, T. Cootes et al. "Automatic Segmentation of the Caudate Nuclei using Active Appearance Models." In Heimann et al. [10], pp. 57–64.
6. K. Li, S. Millington, X. Wu et al. "Simultaneous segmentation of multiple closed surfaces using optimal graph searching." In G. E. Christensen & M. Sonka (editors), *IPMI*, volume 3565 of *Lecture Notes in Computer Science*, pp. 406–417. Springer, 2005.
7. K. Li, X. Wu, D. Z. Chen et al. "Optimal surface segmentation in volumetric images-a graph-theoretic approach." *IEEE Trans. Pattern Anal. Mach. Intell.* **28(1)**, pp. 119–134, 2006.
8. Y. Y. Boykov & V. Kolmogorov. "An experimental comparison of min-cut/max-flow algorithms for energy minimization in vision." *IEEE Trans. Pattern Analysis and Machine Intelligence* **26(9)**, pp. 1124–1137, September 2004.
9. D. Kainmueller, H. Lamecker, S. Zachow et al. "Coupling Deformable Models for Multi-object Segmentation." In F. Bello & E. Edwards (editors), *ISBMS*, volume 5104 of *Lecture Notes in Computer Science*, pp. 69–78. Springer, 2008.
10. T. Heimann, M. Styner & B. van Ginneken (editors). *3D Segmentation in the Clinic: A Grand Challenge*. , 2007.